Experimental and theoretical determination of the Fermi surface of V_3Si

T. Jarlborg, A. A. Manuel, and M. Peter
Département de Physique de la Matière Condensée Université de Genève,
32 Boulevard d'Yvoy, 1211 Genève 4, Switzerland
(Received 4 August 1982)

The Fermi surface of the $A15$ compound V_3Si has been determined by reconstruction from two-dimensional angular correlation of positron annihilation radiation. The Fermi surface is compared to the one obtained from *ab initio* self-consistent linear muffin-tin orbital band calculations and generally good agreement is found to within 2 mRy in the band structure. The results are compared with other experimental and theoretical data.

I. INTRODUCTION

The $A15$ compounds are the subject of various experimental and theoretical studies mainly due to their sometimes very high superconducting transition temperatures. Much insight has been obtained from several electronic structure calculations performed by several different groups during the past few decades.[1-10] On a fine energy scale there are not so many experimental possibilities to test a theoretically determined band structure, especially not away from the Fermi energy E_F. However, the states at E_F can be probed with a high degree of accuracy, and efforts have been made to map the Fermi surface (FS) for some $A15$ compounds by means of de Haas–van Alphen (dHvA) measurements[11,12] and positron annihilation experiments.[13-16] The electron states at E_F are very important for superconductivity, structural transformations, and other properties characteristic of the $A15$ compounds. It is thus very interesting to be able to directly test a calculated FS with that obtained from an experiment.

In this paper we present calculated and measured FS for the high-T_c $A15$ compound V_3Si by use of the self-consistent linear muffin-tin orbital (LMTO) band method and positron annihilation measurements, respectively. Earlier results and descriptions of our methods can be found in Refs. 3 and 16; here we have improved the analysis and focused on the comparison of the FS. Sections II and III describe the band theory and the positron annihilation procedures, respectively, and the result and discussion are presented in Sec. IV.

II. ELECTRONIC STRUCTURE CALCULATIONS

The band structure of V_3Si has been determined by using the LMTO band method.[17] Detailed descriptions of the method of calculation have been given earlier[3,10] for LMTO applications on $A15$ structure calculations. Here we will only mention some important points about the calculations, but especially note and describe differences and improvements over the earlier LMTO calculation of $A15$ compounds.[3]

The calculations are performed self-consistently using spherically symmetric potentials in a geometry of overlapping atomic or Wigner-Seitz (WS) spheres. The basis set is corrected for the overlapping sphere geometry by inclusion of the "combined correction terms"[17] which are of importance for itinerant band states. The basis set includes up to $l=2$ for all atomic sites, with the three center terms including also $l=3$. Thus with eight atoms per $A15$ unit cell the Hamiltonian and overlap matrices are of rank 72, while the structure matrix which includes also $l=3$ is of rank 128. In contrast to the earlier $A15$ calculations the f content ($l=3$) in the wave function is now extracted as intersite tail contributions[3] by using the f terms of the structure matrix.

In a test calculation, a reduced basis was tried by using only s and p basis for the Si sites ($l \leq 1$) to reduce the eigenvalue problem from rank 72 to 62. However, on a fine energy scale (~ 5 mRy) the reduced basis is not sufficient. In particular, the Fermi surface differs from that obtained in the "72-basis" calculation in that the peak in the density of states (DOS) originating from the flat Γ_{12} band is about 4 mRy below the Fermi energy (E_F), while about 2 mRy above otherwise.

The radial wave functions for the valence states are calculated semirelativistically including all relativistic terms except the spin-orbit coupling terms.[18] The core states are fully relativistic and recalculated in each self-consistent iteration. In the earlier calculations the core states were taken from an atomic calculation and frozen throughout the interations. The local density functional of Hedin *et al.*[19] is used

to determine the exchange and correlation contributions to the potential.

A fast canonical band scheme[3] used in the initial stage of the self-consistent procedure gives good starting potentials for the more costly LMTO scheme. Still, one needs usually three or more LMTO iterations to obtain good self-consistent convergence. In these V_3Si calculations about six iterations resulted in a convergence of 2 mRy for states below E_F. The iterations initially used 10 k points in the irreducible Brillouin zone (IBZ), later 20 k points and finally in the last calculation 120 k points. The LMTO calculation working in double precision uses 11 min CPU time per k point on a VAX-780 computer without array processor or floating point accelerator. The compact and energy-independent LMTO basis makes the computation requirements modest compared to other band methods.

From an earlier test of the basis-set convergence in V_3Ga (Ref. 3), it is estimated that the basis used here gives bands below E_F accurately converged to 7 mRy or less. In addition, we have the self-consistence convergence of about 2 mRy. However, these values are given in absolute energy; for the FS topology and structures in the DOS it is the relative energy shifts at different k points which are important. Taking this into account we arrive at smaller uncertainties in the band structure because the major part of the two effects mentioned alter the bands similarly throughout the Brillouin zone BZ. Thus we find that the FS and related band-structure properties have maximum convergence errors of about 2 mRy due to the basis set and self-consistency. On top of this, the band structure has unknown errors due to the use of spherically symmetric potentials, the local-density potential approximation, and the linearization of the band-structure problem. Estimates of these errors are difficult to make. It is through comparison with the positron annihilation data that the accuracy of the obtained band structure will be tested.

The major improvement of this V_3Si band result compared to the earlier LMTO $A15$ calculations[3] is that now the band structure has been determined at 120 k points in the IBZ compared to 35 k points earlier, and that improved k-point integration is used to determine the DOS. This makes it possible to give DOS values within 2 mRy resolution compared to 10 earlier. Two independent methods of k-point integration have been employed: (i) The volume of the IBZ has been divided into tetrahedrons using the *ab initio* 120 regularly spaced k points, and the DOS and number of state functions have been derived analytically for each tetrahedron. This is the commonly used "tetrahedron k-point integration method,"[20] based on the assumption that the bands are linear within each tetrahedron. (ii) A 27-point quadratic interpolation has been used to locally describe the bands analytically around each of the 120 *ab initio* points. From this the energies have been determined in 2024 points in the IBZ followed by a k-point summation to determine the DOS (a 7-point interpolation method interpolating along the x, y, and z directions independently resulted sometimes in poor description of the bands along the [100] and [111] directions). The 27 points are chosen regularly around each *ab initio* k point. At the surfaces, edges, and corners of the IBZ the points are reflected accordingly. The method is convenient to use for any type of structure or BZ, and the band velocities are easily obtained in each point by deriving the analytical expressions for the band structure. It should be mentioned that band crossings have not been considered in the analysis of the band structure.

The $A15$ structure consists of two formula units equal to eight atoms per unit cell. There are two inequivalent WS potentials, one for the six V atoms and one for the two Si atoms. The WS radii differ slightly from what was chosen in the earlier $A15$ calculations and here are $0.307a$ for V and $0.320a$ for Si, where a is the lattice constant 8.923 a.u. These radii give almost the same potential value at the two WS boundaries. Within a reasonable range of WS radii, the band structure is not very sensitive to different choices.[3] The method of calculation employed here has recently been applied to the six V and Nb $A15$ compounds with Ir, Pt, and Au as B elements.[10] The same structure matrices have been used in all these calculations and can be used for other $A15$ materials.

III. ANALYSIS OF THE POSITRON ANNIHILATION DATA

Positrons entering a solid annihilate mainly by emitting two γ rays in nearly opposite directions. The measurements of the lifetime of the positron prior to its annihilation is related to the overlap of the electron and positron wave functions, but in practice it is difficult to extract precise information concerning band structure from such a measurement. On the other hand, the angular correlation of the positron annihilation radiation (ACPAR) is a powerful tool to investigate electron momentum distributions in solids.[21]

If $\rho^{2\gamma}(\vec{p})$ is the momentum density of the photon pair, the basic relation at $T=0$ is

$$\rho^{2\gamma}(\vec{p})=\sum_l \epsilon_l(\vec{p})\sum_{\vec{k}} n_l(\vec{k})\left|\int d^3r\, e^{i\vec{p}\cdot\vec{r}}\psi_+(\vec{r})\times\psi_{\vec{k}l}(\vec{r})\right|^2 . \quad (1)$$

In this expression $n_l(\vec{k})$ is the occupation number of the state $\vec{k}$ in the band, l, $\psi_+(\vec{r})$ is the positron wave function, and $\psi_{k,l}(\vec{r})$ is the electron wave function. $\epsilon_l(\vec{p})$ represents a many-body enhancement which might, according to Ref. 22, vary strongly with the degree of localization of electron states, especially in d metals and alloys. However, the enhancement effects do not change the positions of the FS breaks in $\rho^{2\gamma}(\vec{p})$; thus they will be neglected in this work.

Some positron annihilation experiments on V_3Si were previously reported. The first ones were performed using the standard "long-slit" technique, where one component of $\vec{p}$ is resolved (with a typical resolution of 0.1 a.u.). In this case the measured curve is given by

$$N(p_z) \propto \int_{-\infty}^{\infty} \int_{-\infty}^{\infty} dp_x dp_y \rho^{2\gamma}(\vec{p}) . \tag{2}$$

The first measurement,[13] using a single crystal, showed marked anisotropies. The results were interpreted as hole pockets in the FS and were compared with the prediction of the linear-chain model.[2] Later, a long-slit measurement[14] in the [100] direction was performed. Based on a very elaborated statistical analysis and using a folding procedure equivalent to the Lock, Crisp, and West (LCW) procedure (see below), the authors conclude that planar sections in the FS are present. They discuss their results in the light of the coupled linear-chain model.[1]

With modern machines the measured quantity $N(p_x,p_y)$ is the two-dimensional (2D) projections of $\rho^{2\gamma}(\vec{p})$:

$$N(p_x,p_y) \propto \int_{-\infty}^{\infty} dp_z \rho^{2\gamma}(\vec{p}) . \tag{3}$$

It is only recently that these 2D ACPAR measurements have been introduced,[23–25] and now high resolution (0.035 a.u.) is obtained[26] in both the detection of p_x and p_y. These improvements confer new possibilities to the positron annihilation method which are useful in many fields of solid-state physics.[27]

There are two sets of 2D ACPAR measurements reported on V_3Si.[15,16] Both outline clearly the very large advance obtained by the positron annihilation technique with the use of either multicounter systems or position sensitive γ-ray detectors. Reference 15 reports the results obtained in six crystallographic planes with a geometrical resolution (excluding the smearing due to the residual thermal momentum of the positron) of 0.07×0.21 a.u. These authors reconstruct the momentum distribution and compare it with the FS obtained with the augmented plane-wave (APW) method.[5] The agreement is fairly good but it has to be kept in mind that in one direction the experimental resolution at full width at half maximum (FWHM) is equivalent to 58% of the Γ to X distance, which probably causes a smearing of some structures in the FS topology. These authors have proposed a simple geometrical model for the FS. It consists of two nested hole cylinders along the zone edges and an additional electron density centered about the X point on the zone face; this electron sheet can be either a rectangular box or a cylinder that meets the Γ to R line.

In Ref. 16 we reported 2D ACPAR for two crystallographic planes of V_3Si using a high-resolution apparatus: 0.09×0.10 a.u. at FWHM in which a Gaussian component of 0.05 a.u. at FWHM is included due to the thermal motion of the positron at 77 K. Owing to the small size of the BZ (the edge of the cube is 0.71 a.u.), the increased resolution of these measurements represents an improvement. We want now to describe two analyses used to compare our 2D ACPAR data with the results of the band-structure calculation described in Sec. I.

A. $\vec{p}$- to $\vec{k}$-space remapping

The first approach consists in reducing the measured distributions from $\vec{p}$ space to $\vec{k}$ space. If one assumes that the positron wave function is constant and if the many-body effects are neglected, $\rho^{2\gamma}(\vec{p})$ reduces to $\rho(\vec{p})$, the electron momentum density which is, within the independent particle framework, given by

$$\rho(\vec{p}) = \sum_{\vec{k},l} \sum_{\vec{G}} n_l(\vec{k}) \, | B_{\vec{k},l}(\vec{G}) |^2 \delta(\vec{p}-\vec{k}-\vec{G}) , \tag{4a}$$

with

$$B_{\vec{k},l}(\vec{G}) = \int d\vec{r} \, e^{-i(\vec{k}+\vec{G})\cdot\vec{r}} \psi_{\vec{k},l}(\vec{r}) , \tag{4b}$$

where $\vec{G}$ are the reciprocal-lattice vectors.

The $\vec{p}$- to $\vec{k}$-space remapping is obtained by constructing the following superposition,

$$F(p_x,p_y) = \sum_{P_x,P_y} N(p_x+P_x,p_y+P_y) , \tag{5}$$

where $\vec{P}$ are the reciprocal-lattice vectors expressed in the laboratory coordinate system, i.e., where P_z is parallel to p_z, the integration direction in Eq. (3). This procedure was first introduced by LCW[28] and first used for 2D ACPAR in Ref. 15.

With the use of Eq. (4a) the $F(p_x,p_y)$ superposition can be expressed as

$$F(p_x,p_y) = \int_{\mathscr{P}_z} dp_z \sum_{\vec{P}} \sum_{\vec{k},l} \sum_{\vec{G}} n_l(\vec{k}) \, | B_{\vec{k},l}(\vec{G}) |^2 \times \delta(\vec{p}+\vec{P}-\vec{k}-\vec{G}) . \tag{6}$$

The infinite integration on p_z has been replaced by a sum over all P_z of an integral along $\mathscr{P}_z$, the total path through one Brillouin zone in the considered direction. This equation can be simplified because the $B_{\vec{k},l}(\vec{G})$ coefficients vanish at large $\vec{G}$. Introducing $\vec{H}=\vec{P}-\vec{G}$ one obtains finally,

$$F(p_x,p_y)\propto\int_{\mathscr{P}_z}\sum_{\vec{H}}\sum_{\vec{k},l}n_l(\vec{k})\delta(\vec{p}+\vec{H}-\vec{k})dp_z\ , \tag{7}$$

where the normalization condition has been explicitly taken into account,

$$\sum_{\vec{G}}|B_{\vec{k},l}(\vec{G})|^2=C\ , \tag{8}$$

where C is a constant.

The advantage of constructing the $F(p_x,p_y)$ function from the measured 2D ACPAR is clearly reflected[28] by Eq. (7): We obtain a periodic function which is constant for the filled bands or which reflects the FS topology for bands crossing the Fermi energy.

The main assumption in the $\vec{p}$- to $\vec{k}$-space remapping is for one to consider that the electron momentum density $\rho(\vec{p})$ [Eq. (4)] can be deduced from the momentum density of annihilation of photons $\rho^{2\gamma}(\vec{p})$ [Eq. (1)]. However, it is well known, both theoretically and experimentally, that the low momentum part is more pronounced in $\rho^{2\gamma}(\vec{p})$ and in positron spectra in comparison with $\rho(\vec{p})$ and Compton profiles (see, e.g., Fig. 6 of Ref. 29 for iron). Similar effects may be expected in other transition metals and their alloys. Moreover, even by inclusion of the positron wave function in the independent particle model, the low momentum part of the 1D ACPAR curves is underestimated. However, the position of the FS breaks should be preserved and therefore we assume that, for V_3Si, the FS topology can be brought out by such an analysis. It is, nevertheless, not proved that discrepancies between the measured FS and the calculated one are not due to the assumptions involved in the $\vec{p}$- to $\vec{k}$-space remapping procedure. Particularly, the positron wave function may have some influence on the result but this effect is not known yet; the positron wave function has not been calculated for V_3Si.

The result of this $\vec{p}$- to $\vec{k}$-space remapping has already been reported for our positron annihilation measurements in V_3Si.[16] In this work we compare these experimental $F_{\text{expt}}(k_x,k_y)$, where k_x,k_y are the p_x,p_y values defined within the BZ only, with the model distributions $F_{\text{th}}(k_x,k_y)$, calculated according to Eq. (7), using the occupation number $n_l(\vec{k})$ obtained from the band-structure calculation. Both $F_{\text{expt}}(k_x,k_y)$ and $F_{\text{th}}(k_x,k_y)$ will be presented and discussed in Sec. IV.

B. 3D reconstruction of the occupation number

From Eq. (3) one sees that a 2D ACPAR is the projection of the two-photon momentum distribution in one direction (the normal of the plane containing p_x and p_y). By starting from a set of such projections it is possible to reconstruct the 3D distribution. This problem is encountered in many fields and has been specially investigated in details in nuclear medicine for tomography.[30] Reconstruction from 1D ACPAR is a widely used technique.[31]

In our application, the problem consists of reconstructing the 3D object, i.e., the FS, from its projections on different planes. It is possible to reduce the 3D reconstruction to a set of independent 2D reconstructions by dividing the 3D space in a set of parallel slices and to reconstruct for each of them independently. This procedure, properly speaking, is not a 3D reconstruction, but simplifies the computing effort needed to perform the reconstruction and has already been used successfully.[32] Nevertheless, it imposes a condition to the directions in which the projections may be measured: All these directions must be in a plane. If not, it is not possible to decompose each projection in a set of parallel strips (each strip being uniquely related with one of the slices) defined during the partition of the space where the reconstruction has to be performed.

We have developed a 3D reconstruction technique which avoids this restriction and considers each 2D ACPAR as a function of two variables.[33] Our algorithm is an extension of the usual filtered back-projection operators.[30] It has been explicitly adapted to the case of a crystal with the cubic symmetry. This algorithm can be written as

$$\hat{R}=\sum_{h,k,l}\mathscr{B}_n\{\mathscr{F}_\omega[F_{h,k,l}]\}\ , \tag{9}$$

where $\hat{R}$ denotes the reconstructed density distribution, $\mathscr{B}_n$ the back-projection operator, and $\mathscr{F}_\omega$ the band-limited filtering operator. Let $F_{h,k,l}(\eta,\xi)$ be a two-variables projection. $F_{h,k,l}(\eta,\xi)$ is defined as the integral of $R(\vec{k})$, the (unknown) density distribution, in the crystalline direction $[hkl]$. In our notation, (η,ξ) are the variables in the plane of the particular projection. The first step of the algorithm consists of applying $\mathscr{F}_\omega$, the filtering operator, to each $F_{h,k,l}(\eta,\xi)$. This operator takes first the Fourier transform of $F_{h,k,l}(\eta,\xi)$, then multiplies the Fourier components by a 2D band-limiting convolution function (Ref. 30), ω being the frequency limit and, finally, takes the inverse Fourier transform.

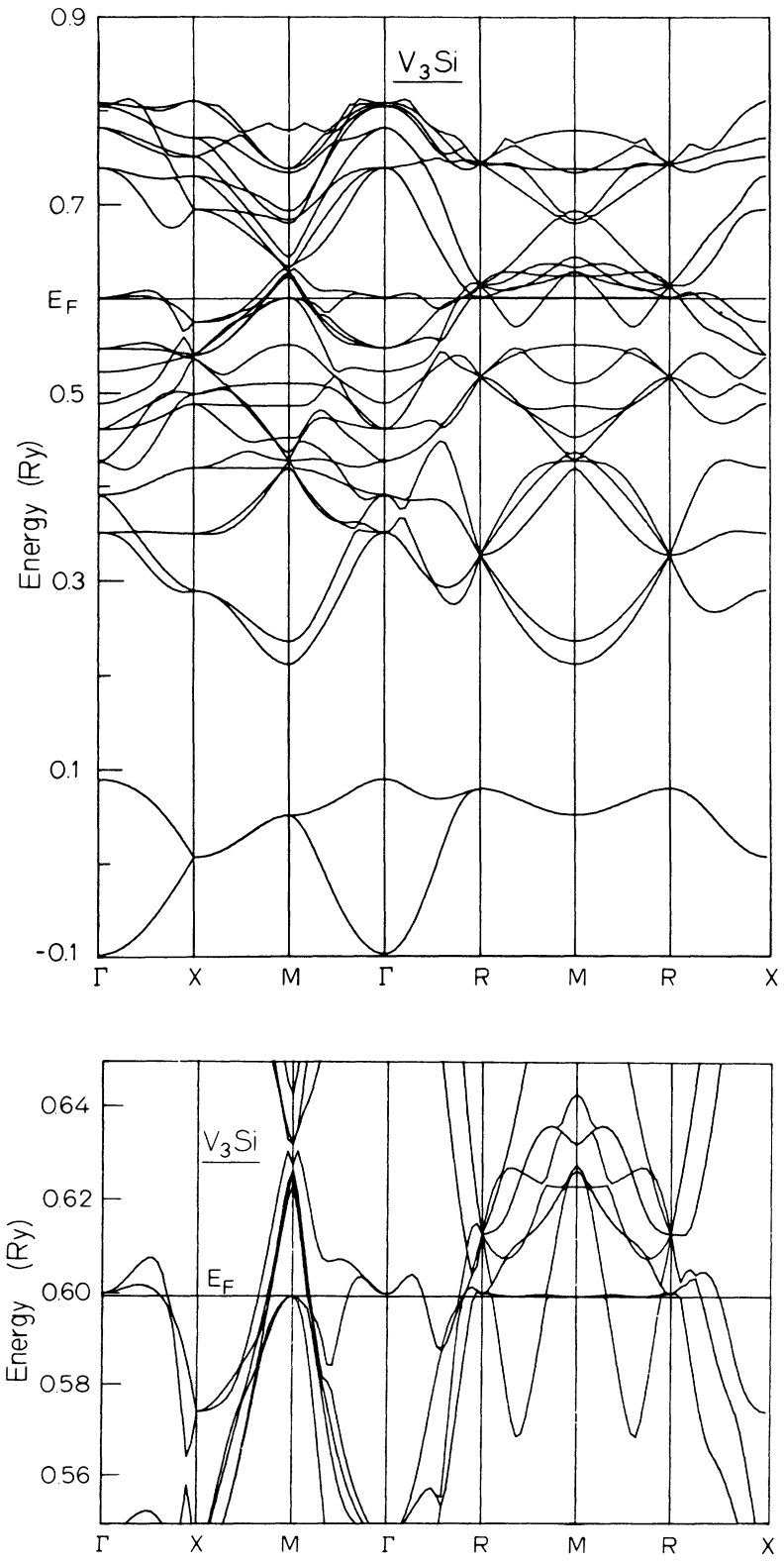

FIG. 1. Self-consistent band structure along symmetry lines for V_3Si obtained from 134 *ab initio* LMTO points. At the bottom a close-up 50 mRy around E_F is shown.

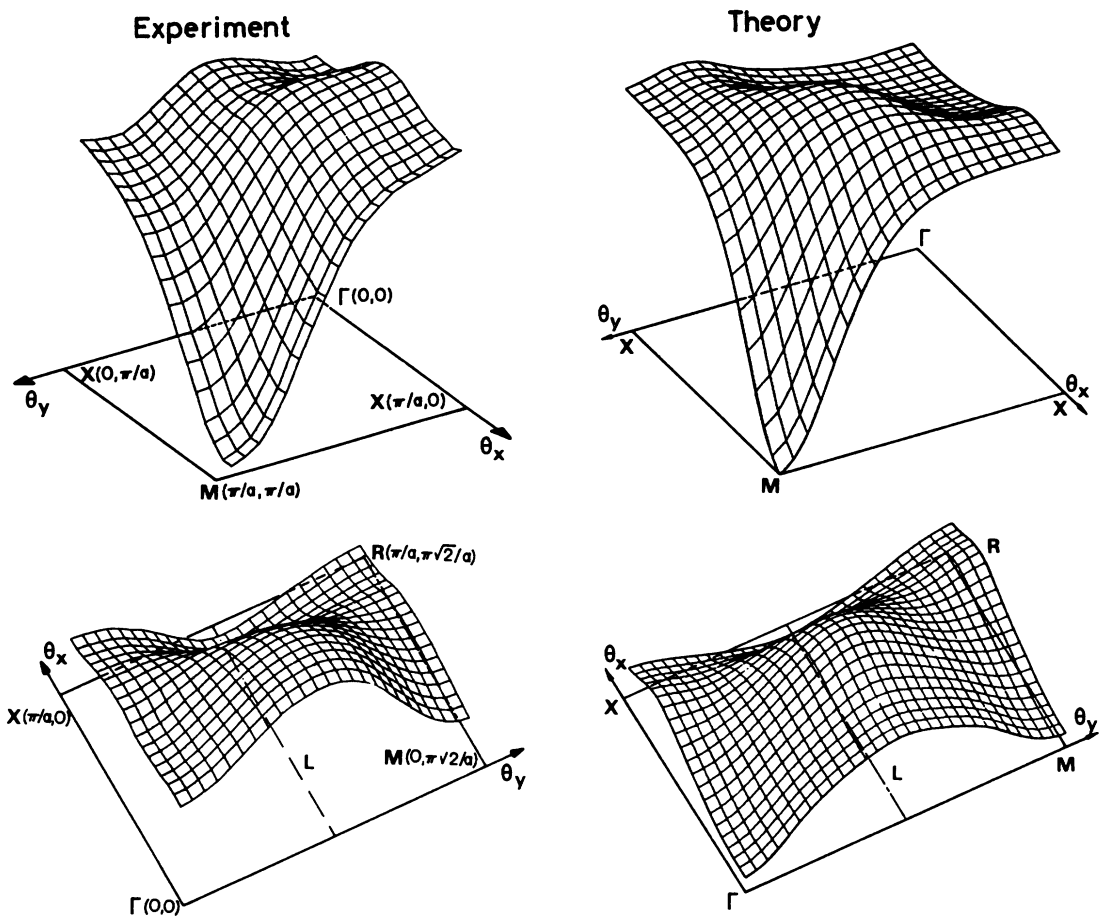

FIG. 2. Reduced-zone representation of 2D ACPAR in V_3Si for two symmetry planes. Upper part (100) plane. Lower part (110) plane. The experimental part (at left) is from Ref. 16.

The second step consists in applying $\mathscr{B}_n$, the back-projection operator. The index n denotes the number of crystalline directions equivalent to $[hkl]$, the back projection is done for each of these n directions. Thus the filtered back-projection algorithm as expressed by Eq. (9) leads us to assume that $\hat{R}$, the reconstructed density distribution, is a good estimate of R, the true density distribution.

We have used this reconstruction scheme to recover the occupation number within the first BZ, starting from a set of two projections $F_{h,k,l}(\eta,\xi)$, where $[hkl]$ are [100] and [110]. These projections were calculated from $N(p_x,p_y)$, the measured 2D ACPAR, according to Eq. (5). Within the two approximations discussed above concerning Eq. (7), this procedure leads us to a distribution $\hat{R}(k)$ for all $\vec{k}$ within the BZ. A constant part can be attributed to the core electrons and to the filled valence bands, but, as the overlap of the positron and electron wave functions has not been calculated, it is not possible to use this constant part of $\hat{R}(\vec{k})$ to scale the reconstructed occupation numbers. Consequently, we have normalized the maximum anisotropy in $\hat{R}(\vec{k})$ to the same value as the maximum anisotropy in the corresponding theoretical distribution: $n(\vec{k})$, which is the total occupation number obtained from our band-structure calculation.

IV. RESULTS

A. Band structure and Fermi surface

The V_3Si band structure is shown in Fig. 1, with a close-up 50 mRy around E_F at the bottom. The figures are drawn directly from 134 *ab initio* points corresponding to 19 intervals between Γ and X, with no band crossings considered. From the close-up one sees that several bands cross E_F thus making the FS quite complicated. At X 20 bands are filled, with 17 at M. At this point a doubly degenerate state is 0.5 mRy below E_F. At Γ, M, and R some bands fall very near E_F making the FS sensitive to small shifts of E_F. Near Γ the band is flat and makes a large contribution to the DOS because it

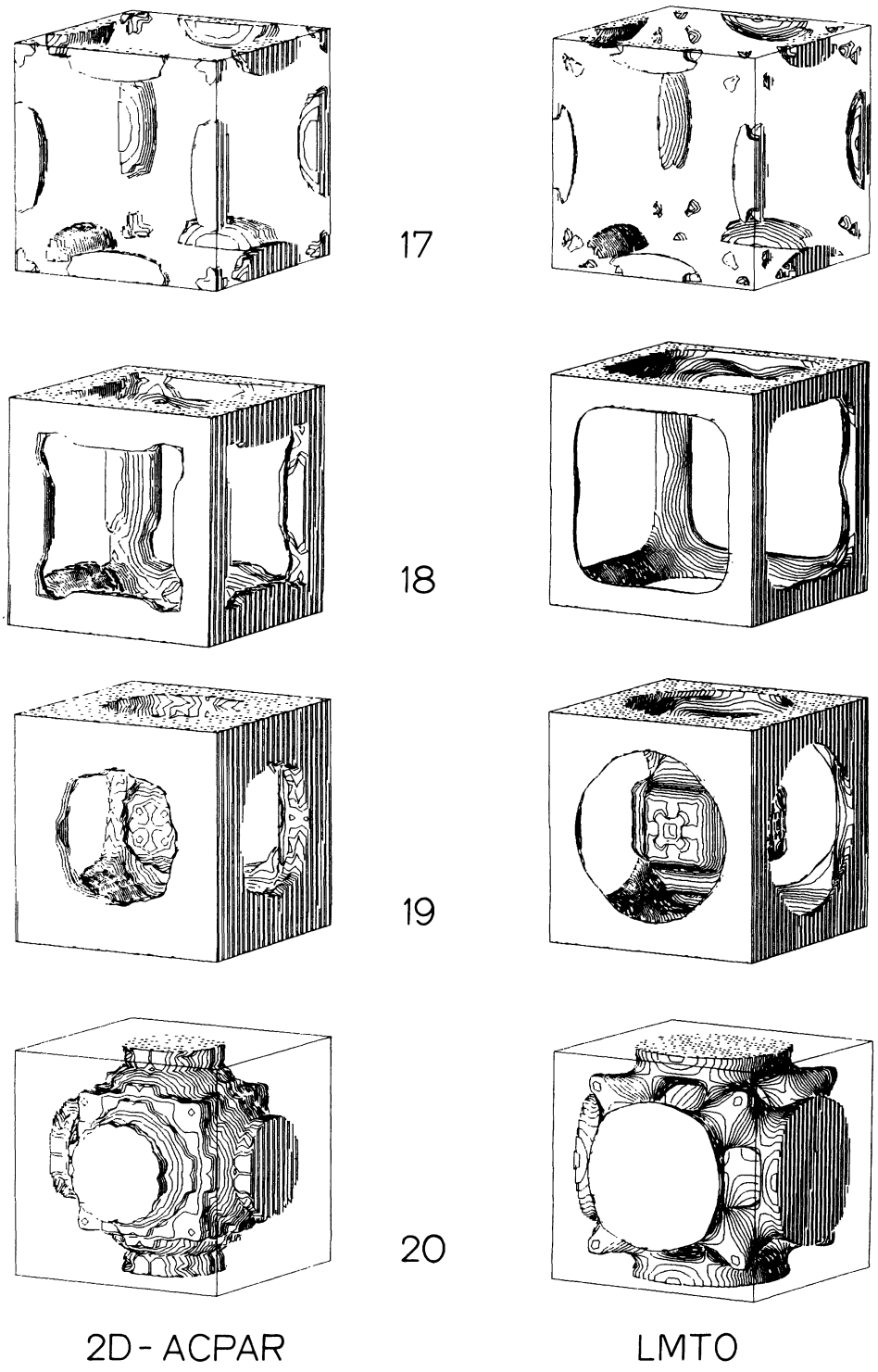

FIG. 3. Right-hand side: The Fermi-surface structures obtained from the four bands which cross E_F (bands 17—20) according to the LMTO band results. For band 17 E_F is raised 2 mRy from the calculated value in order to obtain the M-centered ellipsoids. Left-hand side: The Fermi-surface structures obtained from the 3D reconstructed positron data, by cutting the total yield at four levels corresponding to four bands. The surfaces for bands 17—19 are drawn as hole sheets, while band 20 is drawn as an electron sheet.

covers a large volume. Another extremely flat band coincides with the R-M line and E_F but moves away from E_F as it leaves the R-M region.

In Fig. 2 we show the reduced-zone representation of the 2D ACPAR in V_3Si for two symmetry planes. They were obtained by applying the $\vec{p}$- to $\vec{k}$-space remapping discussed in Sec. III. All the experimental details can be found in Ref. 16. In the same figure the equivalent distribution calculated according to Eq. (7) is shown where the occupation numbers $n(\vec{k})$ have been taken from the band-structure calculation. The agreement is quite good, the general shapes are the same, and this shows already that the LMTO calculation and the positron annihilation results are closely correlated: The depression near Γ in the $XM\Gamma$ plane reflects a hole pocket in the center of the BZ. The large minimum observed at M in the $MX\Gamma$ plane indicates the existence of large hole sheets along the edges of the BZ. Nevertheless, there are two notable differences between the theory and the experiment: Firstly, in the $XM\Gamma$ plane the size of the hole pocket centered at Γ is smaller than in the former. Secondly, in the $RM\Gamma$ plane the amplitude of the theoretical distribution of the reduced 2D ACPAR is smaller at M and at Γ. The points Γ and M are equivalent here because the integration in Eq. (7) projects these two points at the same positions in the (110) plane. These discrepancies will lead to some differences between the calculated FS and the reconstructed one.

In Fig. 3 we show at left the reconstructed positron results where the total yield has been divided into four appropriate levels corresponding to four band crossings with the Fermi energy. In these 3D views we have used the FS plotting routines of Ref. 34. These reconstructed positron results can then directly be compared with the four FS obtained from the band-structure results, shown in the right column of Fig. 3, with that from band 17 at the top to that from band 20 at the bottom. The latter FS is drawn as electrons, the other as holes. In the band-structure FS figures, the Fermi energy is 0.598 Ry as was obtained from the tetrahedron DOS program. However, for band 17, E_F is raised by 2 mRy, which is sufficient to disconnect the M-centered hole ellipsoids from the R points. At 0.598 Ry there is a narrow connection to the R point so that the holes form a thin jungle-gym structure similar to band 18. This very sensitive behavior is due to the very flat band between M and R. Band 19 shows, apart from a jungle-gym structure along the MR edges, a large hole pocket, a box with rounded faces centered around Γ with approximate radius $0.35\bar{a}$, where $\bar{a}$ is the reciprocal-lattice constant. The corresponding "box" is seen in the positron data but is somewhat smaller. On the band structure the box is due to the degenerate band at Γ close to E_F which slowly raises in energy and splits as one goes towards X, turns over, and crosses E_F at about 0.7 of the Γ-X distance $|\Gamma X|$ which is $\frac{1}{2}\bar{a}$. Experimentally, the turnover seems quicker (closer to Γ) due to the smaller dimension of the box. From Γ towards M only one branch crosses E_F at about 0.4 of $|\Gamma M|$, turns, and again crosses E_F together with two other bands closer to the M point. This gives hole pockets around M (part of the jungle gym) of approximate radius $0.12\bar{a}$. Almost circular electron pockets from bands 19 and 20 are found centered at X in the XRM plane with a diameter of about $0.6\bar{a}$, while from the experiment the diameter is smaller, about $0.4\bar{a}$. The dimensions of these orbits can also be read from the band plot as the first E_F crossings around X in the M and Γ directions.

In the band structure FS of band 20 there are "holes" below the M points, as seen in the figure, and they are connected to each other like caves. (They also extend towards Γ and join the box there.) It is not easy to visualize the band behavior behind this structure not seen in the positron data. A band gap due to a neglected band crossing may be the origin. The structure from band 20 has a box around Γ such as for band 19, both in the positron and band data, but in the electron surface plots it is obscured by other structures.

At the Γ point an increase of E_F relative to the bands of only 1 mRy will produce an electron pocket not seen in the positron data. On the other hand, a decrease of E_F of less than 1 mRy gives additional hole pockets at M which might make the hole there too deep in comparison with the positron yield. However, the additional hole would have a very small radius and would be difficult to resolve in the positron data.

Looking at the occupation numbers in the MRX plane, one sees a quite circular electron pocket around X with a radius $0.3\bar{a}$ on top of another squarelike electron pocket two bands below. All this is founded on a larger squarelike electron pocket two bands further down in which the last almost reaches the zone boundary. A better way of describing this is to say there are narrow-hole jungle gyms[15] extending along the MR edges. The mentioned features can be followed on the band plot; for example, along XR two doubly degenerate bands cross E_F approximately halfway. At R four bands are degenerate and coincide with E_F to within 0.5 mRy. Along MR the very flat degenerate band follows E_F very precisely and produces a weak "ridge" at about $\frac{1}{3}$ $|RM|$ from R. (This ridge is avoided by rising E_F 2 mRy as in Fig. 3 for band 17.)

The reconstructed positron data show the same

structures as the calculated occupation numbers. The hole jungle gyms for bands 19 and 20 are thicker than in the band results, which in the band structure would require band crossings with E_F closer to the X point for these bands. A quantitative comparison is difficult to make away from the symmetry points. In addition, we have to realize that this comparison between theory and experiment does not include positron electron matrix elements. Such an inclusion may affect the levels in which the total yield was divided into four FS pieces.

In this context we should also compare our results with those obtained from dHvA measurements. The high T_c in V_3Si makes a complete FS mapping by means of dHvA measurements difficult, but results[11] using pulsed high fields give at least one orbit. This orbit, which is supposed to be an M-centered ellipsoid, is very small, corresponding to an average radius of about 0.07 a.u.$^{-1}$. The M-centered ellipsoid from band 17 has a corresponding extent towards X and Γ while towards R it is larger and also sensitive to small shifts in E_F. (A 2-mRy E_F shift was required to form the ellipsoids from the band structure.) Similar dHvA measurements[12] on the low-T_c $A15$ compound Nb_3Sb showed that the earlier LMTO calculation[3] for this compound was essentially in agreement with the observed orbits except for a 30-mRy band deviation at the M point. The detailed FS of Nb_3Sb is quite different from that of V_3Si, due to one additional filled band making Nb_3Sb a "low-DOS" material. However, shifts of the order of 30 mRy in the calculated V_3Si band structure would cause considerable changes in the FS and be inconsistent with the positron data. Magnetothermal oscillation measurements on the isoelectronic $A15$ compound V_3Ge (Ref. 35) have indicated the presence of three sets of barrel-like sheets oriented similarly to band 17 in Fig. 3. Such structures would result from a lowering of the states at R, relative to the situation in V_3Si, so that the jungle gyms (bands 18 and 19 in Fig. 3) will be disconnected from the R point to look similar to band 17.

By inspecting published band structures of V_3Si obtained by other groups one sees qualitatively that the bands of Refs. 5 and 8 (where the latter is fitted to the former) are similar to ours concerning the hole box around Γ. The bands of interest M and R are a few mRy higher relative E_F than our results which may lead to different FS details, such as larger hole pockets, in this region. The bands of Ref. 2 result in a different FS structure, most notably in an electron pocket around Γ. The states at R coincide with E_F while at M no states are within 10 mRy from E_F. In Refs. 4 and 6 band structures for other $A15$ materials are presented. The bands near E_F for Nb_3Al of Ref. 6 do not look very different from ours for V_3Si, while those for Nb_3Sn of Ref. 4 show an electron pocket around Γ. However, due to the sensitivity of the FS structures, we do not believe that rigid band models or even comparing different isoelectronic $A15$ band structures are accurate ways of FS determination. An example of this is the FS of isoelectronic V_3Si and Nb_3Sn in which the differences are of physical importance.[8] In Ref. 9 the effects of nonspherical corrections to the potential were studied for V_3Si. A reversal of the two states near E_F at the R point was found, otherwise only small effects on states near E_F from nonspherical potential corrections could be found. The reversal of the bands at R so that the fourfold degenerate state is above that of sixfold degenerated differs from most other band results, even those with nonspherical potential corrections.[4,6] The large dispersion of the bands involved near R gives probably only small effects on the FS of such a reversal of states.

B. Other calculated properties

In Fig. 4 we show the DOS for V_3Si obtained from the tetrahedron method. The peak originating from the flat Γ_{12} band is about 2 mRy above E_F. This is in agreement with the nonorthogonal tight-Binding results of Mattheiss and Weber,[8] who fitted the bands to the APW bands of Klein *et al.*,[5] and showed the importance of the position of the Γ_{12} state to explain the martensitic transition in V_3Si. The DOS at E_F is 119 ± 5 states per Ry cell and spin within a 2-mRy energy resolution, which is about 20% larger than that obtained by Mattheiss and Weber. This may be due to the very flat band along MR, which in our case is very near E_F. The earlier LMTO calculation[3] using 10 mRy resolution and using fewer (35 in the IBZ), k points resulted in about 30% lower DOS value at E_F. Our calculated value for the Fermi velocity V_F is $1.3\pm0.1\times10^5$ m/s.

Since we have all the ingredients available to derive electron-phonon coupling λ, superconducting transition temperature T_c, electronic specific-heat coefficient γ, and magnetic exchange enhancement S, we will also present the values obtained. The details of the calculations are exactly the same as were used for six other $A15$ compounds.[10] The electronic numerator in λ is determined using the Gaspari-Gyorffy method,[36] while the phononic denominator has been derived into site contributions using experimentally determined V_3Si phonon moments of Junod *et al.*[37] and the ratio of the pure V and Si Debye temperatures. The superconducting transition temperature is calculated from the McMillan formula[38] with $\omega_{\log}$ from Junod *et al.* The exchange

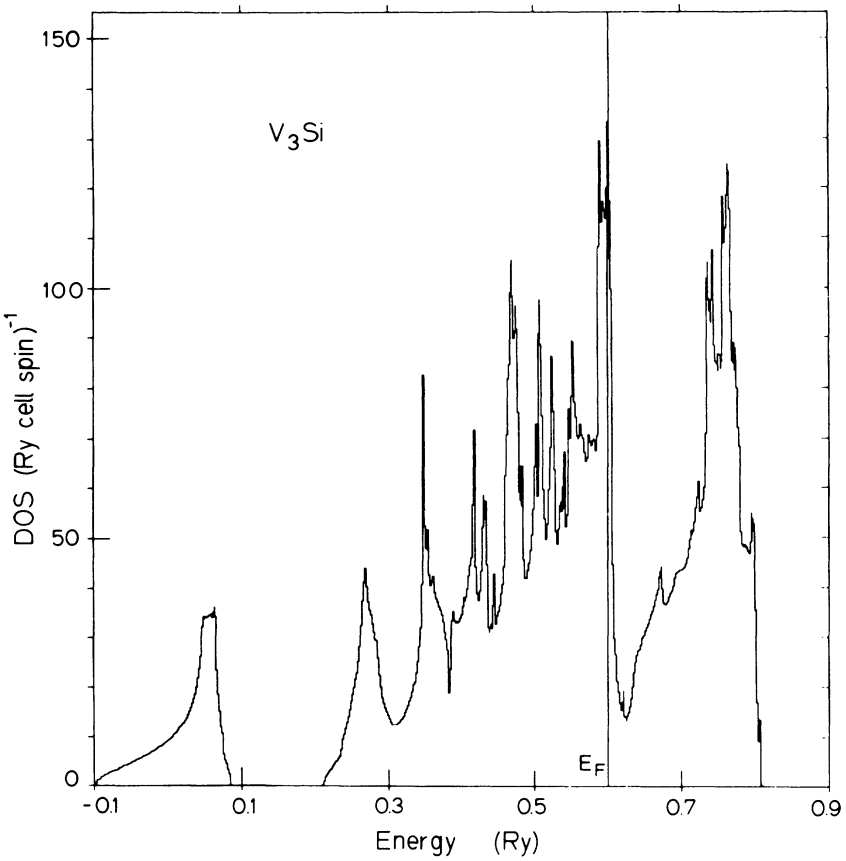

FIG. 4. Total DOS for V_3Si obtained from 120 k points in $\frac{1}{48}$ of BZ using tetrahedron integration method.

enhancement S can be written as $(1-\bar{S})^{-1}$, where the dominant contribution to $\bar{S}$ (as well as to λ) comes from the V atoms.

The relevant quantities involved in the calculations are displayed in Table I together with the results obtained and experimental T_c and γ. The results for T_c and γ are slightly too low but good considering the approximations involved. The deduced $\bar{S}$, about 0.9, is evidently too high; a similar situation was found also for other $A15$ compounds. Spin fluctuations might be of some importance in V_3Si but probably less than in V_3Ga and V_3Au.[10,37]

V. CONCLUSION

The detailed comparison of the V_3Si FS obtained from the *ab initio* self-consistent LMTO band calculation and from 3D reconstruction of 2D ACPAR measurements shows good agreement down to the mRy scale. At several symmetry points where E_F falls near certain bands, it is shown that only 2—3-mRy shifts of E_F lead to evident disagreements between theory and experiment. Such uncertainties are expected from the LMTO results due to incomplete basis convergence, whereas this investigation

TABLE I. Site decomposed phonon moments ω_V and ω_{Si}, electronic contribution to λ, the electron-phonon coupling, the electron-electron interaction parameter μ^*, electronic specific heat γ, superconducting transition temperature T_c, and Stoner parameter $\bar{S}$ as obtained from the band results for V_3Si. Experimental phonon moments ω_{log} and ω_{V_3Si} used in the calculations and experimental γ and T_c are taken from Ref. 37.

ω_{log}	ω_{V_3Si}	ω_V	ω_{Si}					γ		T_c		
		(K)		η_A	η_B			(mJ/K^2 g-at)		(K)		
expt.	expt.			(eV/Å^2)		λ	μ^*	calc.	expt.	calc.	expt.	$\bar{S}$
186	271	226	383	5.8	0.2	1.26	0.18	11.6	14	12.8	17	0.9

has shown that other approximations used in the LMTO calculation are not very important for the FS of V_3Si. The FS structure can be described from the following. Around Γ there are two hole boxes from bands 19 and 20, a small hole ellipsoid is created by band 17 around M, and hole jungle gym structures originating from bands 18–20 envelop the MR lines. The jungle gym is a multiband feature and its details are very sensitive to small shifts in E_F.

ACKNOWLEDGMENTS

We are very grateful to Professor S. Berko, Professor R. M. Singru, Professor P. Descouts, Dr. R. Sachot, Dr. J. Ashkenazi, and Dr. L. Oberli for many discussions. This work was supported by the Swiss National Science Foundation.

[1]M. Weger and I. B. Goldberg, in *Solid State Physics,* edited by H. Ehrenreich, F. Seitz, and D. Turnbull (Academic, New York, 1973), Vol. 28, p. 1.

[2]L. F. Mattheiss, Phys. Rev. 138, A112 (1965); Phys. Rev. B 12, 2161 (1975).

[3]T. Jarlborg and G. Arbman, J. Phys. F 6, 189 (1976); 7, 1635 (1977); T. Jarlborg, *ibid.* 9, 283 (1979).

[4]A. T. van Kessel, H. W. Myron, and F. M. Mueller, Phys. Rev. Lett. 41, 181 (1978); J. Less-Common Met. 62, 49 (1978).

[5]B. M. Klein, L. L. Boyer, D. A. Papaconstantopoulos, and L. F. Mattheiss, Phys. Rev. B 18, 6411 (1978).

[6]W. E. Pickett, K. M. Ho, and M. L. Cohen, Phys. Rev. B 19, 1734 (1979).

[7]V. I. Anisimov, V. A. Gubanov, A. L. Ivanovskii, E. Z. Kurmaev, J. Weber, and R. Lacroix, Solid State Commun. 29, 185 (1979).

[8]L. F. Mattheiss and W. Weber, Phys. Rev. B 25, 2243 (1982).

[9]L. F. Mattheiss and D. R. Hamann, Solid State Commun. 38, 689 (1981).

[10]T. Jarlborg, A. Junod, and M. Peter, Phys. Rev. B 27, 1558 (1983).

[11]A. J. Arko, D. H. Lowndes, F. A. Muller, L. W. Roeland, J. Wolfrat, A. T. van Kessel, H. W. Myron, F. M. Mueller, and G. W. Webb, Phys. Rev. Lett. 40, 1590 (1978).

[12]A. J. Arko, G. W. Crabtree, and Z. Fisk, in *Superconductivity in d- and f-band Metals,* edited by H. Suhl and M. B. Maple (Academic, New York, 1980), p. 87.

[13]S. Berko and M. Weger, Phys. Rev. Lett. 24, 55 (1970); Phys. Rev. B 4, 521 (1972).

[14]S. Samoilov and M. Weger, Solid State Commun. 24, 821 (1979); S. Samoilov, M. Weger, I. Nowik, I. B. Goldberg, and J. Ashkenazi, J. Phys. F 11, 1281 (1981).

[15]W. S. Farmer, F. Sinclair, S. Berko, and G. M. Beardsley, Solid State Commun. 31, 481 (1979); S. Berko, W. S. Farmer, and F. Sinclair, in *Superconductivity in d- and f- Metals,* edited by H. Suhl and B. Maple (Academic, New York, 1980), p. 281; S. Berko, in *Positron Annihilation,* edited by R. R. Hasiguti and K. Fujiwara (The Japan Institute of Metals, Sendai, 1979), p. 65.

[16]A. A. Manuel, S. Samoilov, R. Sachot, P. Descouts, and M. Peter, Solid State Commun. 31, 955 (1979); *Superconductivity in d- and f- Metals,* edited by H. Suhl and B. Maple (Academic, New York, 1980), p. 273.

[17]O. K. Andersen, Phys. Rev. B 12, 3060 (1975).

[18]D. D. Koelling and B. N. Harmon, J. Phys. C 10, 3107 (1977).

[19]L. Hedin, B. I. Lundqvist, and S. Lundqvist, Solid State Commun. 9, 537 (1971).

[20]J. Rath and A. J. Freeman, Phys. Rev. B 11, 2109 (1975); O. Jepsen and O. K. Andersen, Solid State Commun. 9, 1763 (1971); G. Lehmann and M. Taut, Phys. Status Solidi B 54, 469 (1972).

[21]*Positron Solid State Physics,* edited by W. Brandt and A. Dupasquier (North-Holland, Amsterdam, 1983).

[22]See, for example, M. Sob, J. Phys. F 12, 571 (1982); P. E. Mijnarends, and R. M. Singru, Phys. Rev. B 19, 6038 (1979).

[23]S. Berko, M. Haghgooie, and J. J. Mader, Phys. Lett. 63A, 335 (1977).

[24]A. A. Manuel, S. Samoilov, Ø. Fischer, and M. Peter, Helv. Phys. Acta 52, 255 (1979).

[25]R. N. West, J. Mayers, and P. A. Walters, J. Phys. E 14, 478 (1981).

[26]P. E. Bisson, P. Descouts, A. Dupanloup, A. A. Manuel, E. Perréard, M. Peter, and R. Sachot, Helv. Phys. Acta 55, 100 (1982).

[27]*Positron Annihilation,* edited by P. G. Coleman, R. C. Sharma, and L. M. Diana (North-Holland, Amsterdam, 1982).

[28]D. G. Lock, V. H. C. Crisp, and R. N. West, J. Phys. F 3, 561 (1973); R. N. West, in *Physics of Transition Metals, 1980,* edited by P. Rhodes (Institute of Physics, Bristol, 1981), p. 35.

[29]W. C. Phillips and R. J. Weiss, Phys. Rev. B 6, 4213 (1972).

[30]R. A. Brooks and G. Di Chiro, Phys. Med. Biol. 21, 689 (1976) and G. T. Herman, S. W. Rowland, and M. Yau, IEEE Trans. Nucl. Sci. NS-26, 2879 (1979).

[31]P. E. Mijnarends, in *Compton Scattering,* edited by B. Williams (McGraw-Hill, New York, 1977), p. 323.

[32]See contributions of S. Berko in Refs. 15, 21, and 27, and L. M. Pecora and A. C. Ehrlich, R. L. Waste and R. N. West, and G. Kontrym-Sznajd in Ref. 27.

[33]A preliminary description of this method is given in A. A. Manuel, Phys. Rev. Lett. 49, 1525 (1982).

[34]P. C. Pattnaik, P. H. Dickinson, and J. L. Fry, Comput.

Phys. Commun. 25, 63 (1982).
[35]J. E. Graebner and J. E. Kunzler, J. Low Temp. Phys. 1, 443 (1969).
[36]G. D. Gaspari and B. L. Gyorffy, Phys. Rev. Lett. 28, 801 (1972).
[37]A. Junod, T. Jarlborg, and J. Muller, Phys. Rev. B 27, 1568 (1983).
[38]W. L. McMillan, Phys. Rev. 167, 331 (1968).